Combustion and Flame 198 (2018) 455–465

Contents lists available at ScienceDirect

Combustion and Flame

journal homepage: www.elsevier.com/locate/combustflame

# Improvement and validation of a detailed reaction mechanism for thermal decomposition of RDX in liquid phase

Mayank Khichar, Lalit Patidar, Stefan T. Thynell*

*Department of Mechanical and Nuclear Engineering, The Pennsylvania State University, University Park, PA 16802, USA*

ARTICLE INFO

*Article history:*
Received 17 May 2018
Revised 17 June 2018
Accepted 4 October 2018

*Keywords:*
Liquid-phase decomposition
Reaction mechanism
Quantum mechanics
RDX
Dominant decomposition pathway

ABSTRACT

The objective of this work is to validate an expanded version of a recently developed reaction mechanism describing liquid-phase decomposition of RDX. The validation involves a comparison of experimental results obtained from confined rapid thermolysis at various set temperatures. In the experiments, the decomposition occurs in the liquid phase, which results in evolution of species into the gas phase. The spectral transmittances of the gas-phase species are measured using FTIR spectroscopy, and these spectra are processed to obtain the temporal behavior of the evolved species using the HITRAN data base. A species conservation model was developed to simulate the confined rapid thermolysis experiments. The model incorporates the detailed liquid-phase reaction mechanism. The rate parameters in the reaction mechanism were optimized by comparing the experimental and computational results. With the optimized parameters, the computational model reproduces the experimentally observed trends with reasonable accuracy. Some of the deviations can be explained by experimental uncertainty. Based on the use of the computational model, initiation of decomposition occurs by HONO elimination. The subsequent decomposition occurs via the pathway starting with HONO addition and followed by ring opening. The detailed reaction mechanism containing 321 species and 500 elementary reactions was reduced to 53 species and 56 reactions using a sensitivity analysis.

© 2018 The Combustion Institute. Published by Elsevier Inc. All rights reserved.

## 1. Introduction

Cyclotrimethylenetrinitramine (RDX) is a common ingredient in rocket propellants and explosives. It belongs to the class of cyclic-nitramine explosives, such as, octahydro-1,3,5,7-tetranitro-1,3,5,7-tetrazocine (HMX). Many experimental and computational efforts have been made to elucidate the thermal decomposition of cyclic nitramines [1,2]. A critical analysis of such decomposition and its products has been reviewed [3–5]. A better understanding of the thermal decomposition can help to create useful models for predicting combustion instability, impact sensitivity, electrostatic discharge, and burning rate behavior. Additionally, a thorough knowledge of cyclic-nitramine decomposition behavior may assist the development of newer and safer propellants for long-term storage.

The initial decomposition model for RDX and HMX in the gas phase was developed by Melius [6] using quantum chemical bond-additivity-corrected Moller–Plesset fourth-order perturbation theory method (BAC-MP4). Melius' model also included data from a generalized hydrocarbon/air flame model of Miller et al. [7–9]. Alexander et al. [10] recognized the inability of BAC-MP4 method to treat the reaction coordinate for the bond breaking of cyclic-nitramines to form $NO_2$, or its recombination, and suggested further development of Melius' model. The gas-phase reaction mechanism was later refined by Yetter et al. [11] by considering reactions among the smaller molecular weight species, such as $CH_2O$, $N_2O$, $NO_2$, $H_2$, HCN, and NO. Chakraborty et al. [12] performed density functional theory (DFT) calculations at B3LYP/6-31G(d) level of theory [13] to further enhance the reaction mechanism. In particular, successive HONO elimination reactions were emphasized. Litzinger et al. [14] modeled gas-phase decomposition of RDX and validated Yetter's mechanism by reproducing experimental species mole fractions using the CHEMKIN II software [15–17] with the PREMIX subroutine [18]. Liau and Yang [19] used the gas-phase mechanism by Yetter et al. [11] in their combustion model to predict burn rate, temperature and species profiles in the 1-90 atm pressure range. In a subsequent study by Anderson and Conner [20], a combustion model was developed with the main objective of comparing the gas-phase mechanisms by Yetter et al. [11] and Chakraborty et al. [12]; condensed-phase reactions were not considered. Burning rates calculated using either of the mechanisms agreed with the experimental results. However, neither mechanism was able to completely reproduce the experimentally

* Corresponding author.
*E-mail address:* thynell@psu.edu (S.T. Thynell).

https://doi.org/10.1016/j.combustflame.2018.10.005
0010-2180/© 2018 The Combustion Institute. Published by Elsevier Inc. All rights reserved.

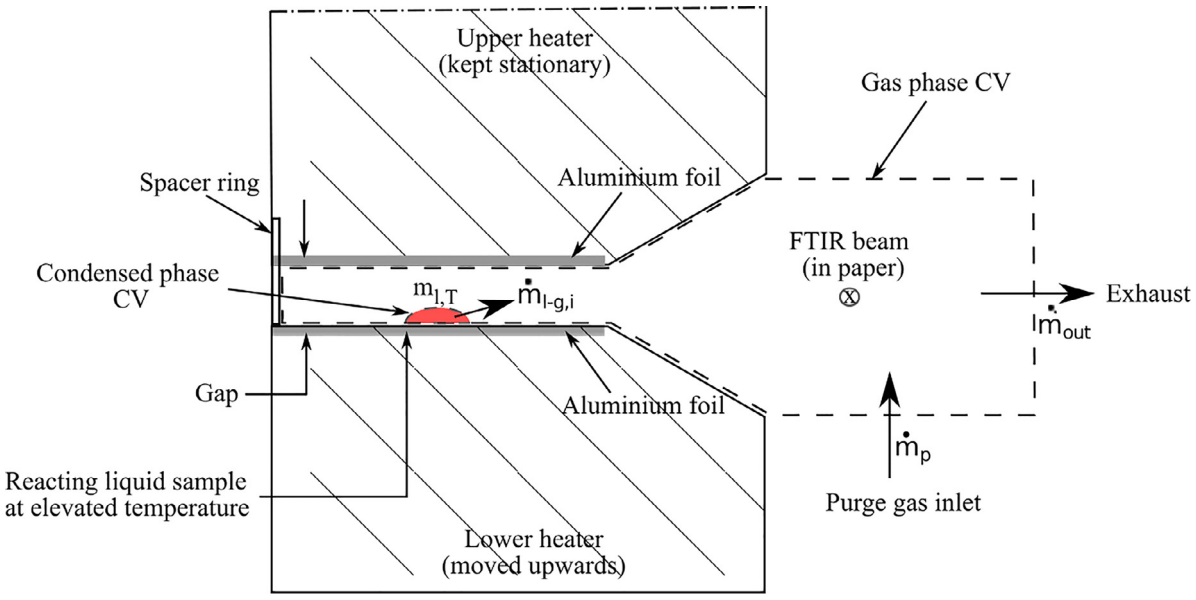


**Fig. 1.** Schematics of the thermolysis chamber and the accessories required for species detection in gas phase.

obtained trace species profiles. This inadequacy was attributed to a limited knowledge of the extent of condensed-phase reactions.

Condensed-phase global mechanisms for cyclic-nitramines were developed by Brill et al. [21], Tarver et al. [22], Hobbs [23] and Behrens [24]. In several combustion models developed for cyclic nitramines, the global mechanism for condensed phase was used along with the detailed gas-phase mechanism [1,19,25–27]. However, a global mechanism is unlikely to capture the complex decomposition process of cyclic-nitramines in the condensed phase. Hence, there is a need to develop a comprehensive condensed-phase reaction mechanism with reliable chemical kinetics data. Since an experimental determination of a detailed mechanism is a challenging task, a complementary quantum-mechanics (QM) based approach is adopted. Fortunately, QM calculations have improved significantly to the level that liquid-phase reactions can be identified.

Recently, Patidar and Thynell [28] and Patidar et al. [29] used QM calculations to identify the initiation pathways for liquid-phase decomposition of RDX and HMX, respectively. Patidar and Thynell [28] investigated the four experimentally obtained pathways by Behrens and Bulusu [30] and presented a detailed chemical kinetics mechanism consisting of five decomposition pathways for RDX. Similarly, Patidar et al. [29] examined the four experimentally obtained pathways by Bulusu and Behrens [31] and presented a detailed chemical kinetics mechanism consisting of five decomposition pathways for HMX.

The objective of the current study is to expand and validate the liquid-phase decomposition mechanism of RDX proposed by Patidar and Thynell [28] by using experimental results from confined rapid thermolysis. In the expanded mechanism, many secondary reactions were identified to link intermediate species to the final decomposition products detected in the experiments. Specifically, several important reactions among the smaller molecular weight species, such as CO, $CO_2$, $CH_2O$, NO, $NO_2$, $CH_2NH$, HONO, HCOOH, etc., were added to the mechanism. For its validation, the developed liquid-phase reaction mechanism for RDX is included in a transient model simulating the confined rapid thermolysis experiment, covering the temperature range from 538 to 568 K. A sensitivity analysis is performed to identify the most important reactions, which also yields a reduced reaction mechanism.

## 2. Experimental details

To study the thermal decomposition of RDX in the liquid phase, we employ results from confined rapid thermolysis [32]. In this experiment, a sub-milligram sample is rapidly heated (2000 K/s) to a set temperature where decomposition occurs under constant pressure condition [33]. The spectral transmittance of the evolved gases is recorded by an FTIR spectrometer operating at a 2.6 $cm^{-1}$ wavenumber resolution. A transmittance spectrum is recorded every 50 ms, covering the spectral range from 600 to 3750 $cm^{-1}$. The evolved decomposition products enter a cool atmosphere, which is purged by with an inert gas ($N_2$); thus gas-phase reactions among the evolved decomposition products are very limited and neglected. The schematics of the thermolysis region with position of RDX sample is shown in Fig. 1. A detailed explanation of the setup and experimental procedure is provided by Chowdhury and Thynell [32] and is not repeated here. Schematics of FTIR system and accompanying optics is provided in [34]. Using a measurement period of about 7 seconds, 350 spectra were recorded.

## 3. Data reduction procedure

Multiple thermolysis experiments were performed at each set temperature and at atmospheric pressure. To quantify the species concentration, each spectrum was analyzed separately using a data-reduction model described in [34]. The model relates the species concentrations with measured spectral transmittance assuming validity of Beer's law. It takes into account the finite spectral resolution of the spectrometer [35]. The measured transmittance is obtained by a convolution of the true transmittance with the instrument line shape over the entire wavenumber range. The true transmittance of the gaseous mixture depends on the species concentrations along with the overlap of spectral lines from same and different species. The required radiative properties of the IR active species were taken from the HITRAN database [36].

The data-reduction model was solved using an inverse routine implemented in [37]. The merit function $\chi^2$, defined as the difference between the experimental and the theoretical spectral transmittance, was minimized. The computational procedure requires specification of the total pressure, gaseous mixture temperature, optical path length, guessed partial pressures, and the

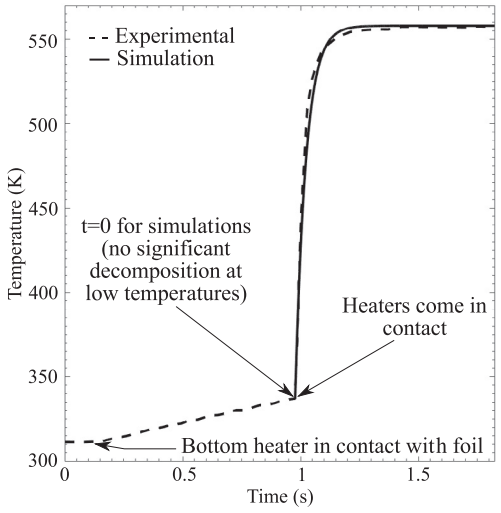


**Fig. 2.** Variation of sample temperature in the CRT experiment and computational model for a set temperature of 558 K and 1 atm pressure.

spectral range. Species considered for the data reduction process were selected based on the experimentally obtained IR spectrums. Table S1, included in the supplementary material, shows the list of identified species, where the spectral ranges were obtained from the NIST webbook [38]. The selection of spectral ranges for quantification of species concentrations was based on careful consideration of spectral range overlaps. In an overlap region, less sensitive species may go undetected or the model can give erroneous results. Hence, the spectral overlaps regions were avoided for analysis wherever possible. The selected spectral regions are shown in Table S1. On the successful convergence of the model for a particular spectrum the relative concentrations of $NO_2$, NO, CO, $N_2O$, $CO_2$, $CH_2O$, HCN, and $H_2O$ are obtained at the corresponding time instant. The obtained concentration values are considered as relative because of the uncertainty in optical path length. A value of 1 cm for optical path length was assumed for the calculations.

## 4. Experimental results

### 4.1. Sample temperature during decomposition

The temperature of the sample in its liquid state is approximated by the temperature measured by a 75 μm K-type thermocouple placed between aluminum foil and heater. The obtained variation for a set temperature of 558 K is shown in Fig. 2. Sample temperature starts increasing in an approximately linear fashion when the bottom heater comes in contact with the aluminum foil, in contact with the thermocouple. This slow increase in sample temperature continues till the two heaters come in contact with each other. In this low-temperature region, the RDX decomposition rate is minimal and can be ignored without any significant loss of accuracy in simulation results. When the bottom heater comes in contact with the stationary top heater, the sample temperature increases quickly at a rate of about 2000 K/s. In approximately 0.18 s sample temperature reaches within 10 °C of the set temperature and then converges asymptotically. This variation in sample temperature for the time interval in which the two heaters are in contact can be approximated by an exponential function. The optimized exponential function to mimic the experimental behavior of sample temperature $T$ is given by,

$$T = T_{set} - (T_{set} - T_i)\exp\left(-\frac{t}{\tau}\right), \tau = 0.045\,s \quad (1)$$

where, $T_{set}$ is set temperature of the sample, $T_i$ is initial sample temperature, $\tau$ is time constant, and $t$ is time in seconds. This function was provided as input to the computational model for thermal decomposition process of RDX at different set temperatures. Figure 2 shows the comparison between experimental and computational sample temperatures. The overlap with experimental temperature shows a maximum deviation of ~5 K for less than 0.5 s.

### 4.2. IR spectrum of gas-phase species

Figure 3 shows a single transmittance spectrum with bands corresponding to different product species for a set temperature of 558 K. The spectrum was obtained at $t = 4.84$ s from the start of the decomposition process. The different bands present in the spectrum indicate the presence of $N_2O$, $NO_2$, NO, HCN, $CH_2O$, $CO_2$, CO, and $H_2O$ in significant concentrations. These species match with the earlier identified products of RDX decomposition by Schroeder [5] and Oyumi and Brill [39]. According to Beer's law, the band height depends upon the species concentration and its molar absorptivity. CO and NO are less IR-active due to a low value of their permanent dipole moments, and hence their bands are weak. Many other similar species can be present in the gas phase and are not identified here. For the current study, we only focus on the evolution of these eight species.

### 4.3. Concentration of gas-phase species

The model described in Section 3 was applied to each of the acquired spectrums to provide species relative mole fractions at corresponding time instants. These relative mole fraction values at different time instants were combined together to create profiles for the entire 7 s interval of an experiment. These relative mole fraction profiles were obtained for set temperatures of 538 K, 548 K, 558 K, and 568 K. Figure 4 shows the relative mole fraction profiles of all the eight identified product species for the set temperature of 568 K. Even though the set temperature varies from 538 to 568 K, the species evolution rates vary significantly.

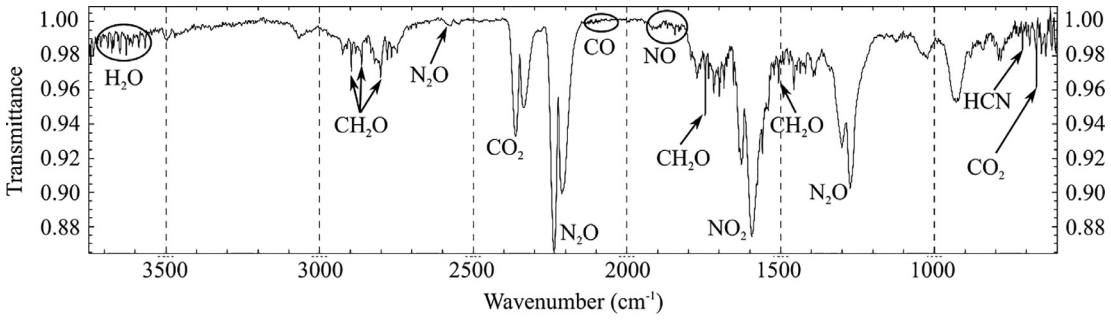


**Fig. 3.** IR spectrum of species in gas-phase region evolved during RDX decomposition for a set temperature of 558 K and 1 atm pressure.

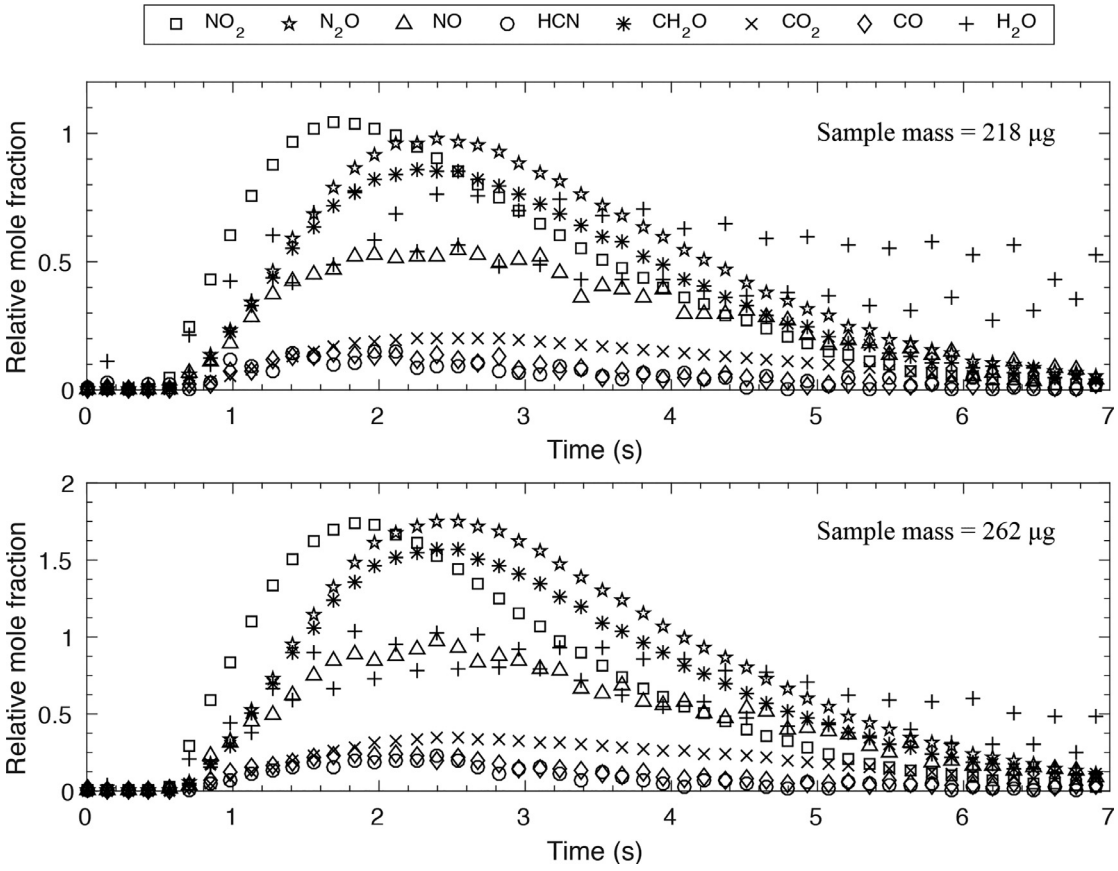


**Fig. 4.** Temporal species evolution for two experiments with slightly different sample masses at a set temperature of 568 K and 1 atm pressure.

To get a qualitative estimate of the uncertainty in the experimentally obtained relative mole fraction profiles, three experiments were performed at each set temperature. For these experiments, all other experimental parameters such as purge gas flow rate and pressure were kept constant except sample mass. Since the sample mass was in micrograms, it was not possible to exactly use the same amount every time. The variation in experimental relative mole fraction profiles for two experiments performed at a set temperature of 568 K is shown in Fig. 4. For these two experiments, the initial mass of RDX sample was slightly different (218 μg and 262 μg). The sample with more mass is expected to release more gaseous products upon decomposition. However, the evolution of different species relative to each other is expected to remain largely the same. Figure 4 shows that for the sample with 262 μg initial mass the relative mole fractions of evolved species are slightly higher. The relative mole fraction profiles corresponding to the two initial sample masses are, however, not exactly same. For the sample with 218 μg of initial mass of RDX, $NO_2$ peak is higher than $N_2O$ peak but for the sample with 262 μg of initial mass $N_2O$ peak is slightly higher than $NO_2$ peak. Similar variations are obtained for other species as well at other temperatures. These results suggest that the experimentally obtained relative mole fractions have an uncertainty of approximately 10%. From Fig. 4, it can also be observed that the relative mole fraction value for $H_2O$ fluctuates much more than other species. These fluctuations are not physically possible. It suggests that the data reduction model results for $H_2O$ are much less reliable compared to other species. In general, these large variations in $H_2O$ concentration are caused by its fine line structure, which is very difficult to resolve. For example, in the works by Brill and co-workers [39,40], the evolution of $H_2O$ is not estimated; only the initial appearance of $H_2O$ is given. To improve the quality of the predictions, it is necessary to increase the spectral resolution, but it comes at the expense of a decreased time resolution and increased noise in the spectra.

Figure 4 also shows that $NO_2$ emerges quickly in the initial phase of decomposition, reaches its peak value and then decreases. NO seems to roughly follow $NO_2$ evolution trend although the peaks are somewhat shifted. This suggests that most major pathways of their production are common. Similarly, the relative mole fraction profiles for $N_2O$ and $CH_2O$ follow almost the same trend. Both species emerge at a slightly lower rate than $NO_2$ during the initial decomposition phase, reaches peak value and then decreases. The peaks for these two species occur after the peak of $NO_2$. The evolution profiles of $CO_2$ and CO follow almost the same trend with a small difference in their absolute concentration values. The concentrations of $CO_2$, CO, and HCN are small compared to other species.

The effect of the set temperature on RDX decomposition process in liquid phase was also studied. Relative mole fraction profiles obtained for set temperatures in the range 538–568 K were compared. It was observed that with increase in set temperature, the peaks in the relative mole fraction profiles of all the species become higher and emerge earlier in the decomposition event. Also, the $NO_2$ mole fraction relative to $N_2O$ increases as the set temperature increases. Similar trend of $NO_2/N_2O$ ratio was obtained by Brill and co-workers [40,41] in their experimental work on explosives and propellants, including RDX and HMX.

## 5. Model for decomposition of RDX

A species conservation model, similar to the model by Lee and Litzinger [42], was developed to validate our RDX liquid-phase decomposition mechanism. The model consists of three key components, (1) liquid-phase reaction mechanism, (2) conservation

equations for mass and species in the liquid-phase region, and (3) conservation equations for mass and species in the gas-phase region. Each one is described in following sub-sections.

### 5.1. Liquid-phase reaction mechanism

The liquid-phase decomposition mechanism of RDX, recently developed by Patidar and Thynell [28], was further augmented in the current study. Several secondary reactions were added by following the same approach that was utilized by Patidar and Thynell [28] and is summarized briefly here.

Elementary reactions were identified from QM calculations using Gaussian 09 quantum chemistry software package [43]. Density functional theory (DFT) was used with the hybrid functional B3LYP [13]. This hybrid functional provides sufficient accuracy in energy calculations of stable species and transition states [12,44]. The basis set 6-311++G(d,p) was used to perform geometry optimization calculations for reactants, products, and transition states. These calculations were used to obtain equilibrium and transition state properties required for rate kinetics. The conductor-like polarizable continuum model (CPCM) [45] was used as solvation model with water as the solvent. The choice of solvation model and the solvent was justified by Patidar and Thynell [28] after comparing the three solvation models, IEFPCM [46], SMD [47], and CPCM, with water, acetonitrile, and diethyl ether as solvents. The CPCM model is parametrized to give accurate free energy of solvation values at 298 K, but has an inherent mean unsigned error of 4–5 kcal/mol depending on whether neutral or ionic species are considered. In addition, intrinsic reaction coordinate calculations were also performed to connect the reactants to the products via the identified transition state. In general, the default parameters were used in the Gaussian program package. All calculations were performed at 298 K due of the unavailability of a computer program that allows evaluation of free energy at elevated temperatures in the liquid phase.

### 5.2. Analysis of liquid-phase region

The liquid-phase model is formulated based on the conservation equations of mass and species. The control volume (CV) for this model is defined by the boundaries of the sample present in the liquid phase, shown in Fig. 1. The CV is sandwiched between two heaters 300 μm apart. For such a small CV, it is reasonable to ignore the small concentration gradients for the species within the liquid sample. Hence, the transient mathematical model for the liquid-phase is zero-dimensional.

The temporal evolution of a species inside this CV can be attributed to its net production rate via chemical reactions and rate of evaporation. The net evaporation rate of species $i$ can be expressed as, $\dot{m}_{lg,i} = m_{l,i} k_{lg,i}$ where, $m_{l,i}$ is its mass in liquid phase and $k_{lg,i}$ is its liquid-to-gas conversion rate constant, expressed in an Arrhenius form. The net mass production rate of species $i$ due to all elementary reactions can be expressed as, $\dot{m}_{rxn,l,i} = (\dot{\omega}_{l,i} W_i/\rho_l) m_{l,T}$, where $\dot{\omega}_{l,i}$ is the net molar production rate per unit volume, $W_i$ is the species molecular weight, $\rho_l$ is the liquid-phase density, and $m_{l,T}$ is total mass of the liquid phase. For the experimentally measured sample temperature range, the density of the liquid sample is assumed constant. Hence, the set of mass conservation equations which governs the temporal evolution of species mass fraction $Y_{l,i}$ in the liquid phase is given by,

$$\frac{d}{dt}\left(Y_{l,i}\right) = \frac{\dot{\omega}_{l,i} W_i}{\rho_l} - Y_{l,i} k_{lg,i} + Y_{l,i} \sum_{j=1}^{n_g - 1} Y_{l,j} k_{lg,j}, \quad i = 1,\ 2,\ \ldots,\ n_l \tag{2}$$

where, $n_l$ and $n_g$ are the total number of species in liquid and gas phase, respectively.

$\dot{\omega}_{l,i}$ can be evaluated by considering rate law and species stoichiometry for each of the elementary reactions of species $i$. The effective rate constant $k_{eff}$ for an elementary reaction is evaluated using kinetics-based ($k_{kin}$) and diffusion-based ($k_{diff}$) rate constants,

$$\frac{1}{k_{eff}} = \frac{1}{k_{kin}} + \frac{1}{k_{diff}}. \tag{3}$$

The kinetics-based rate constants are evaluated using the thermodynamic formulation of conventional transition state theory [48], expressed as

$$k_{kin,f}(T) = \sigma_s\ \tau_{tun} \frac{k_B T}{h\ c_{ref}^{n-1}}\ \exp\left(-\frac{\Delta G_f^{\ddagger}}{R_u T}\right) \tag{4}$$

where, $k_B$ is the Boltzmann constant, $h$ the Planck's constant, $R_u$ the universal gas constant, $n$ the order of the reaction, and $c_{ref}$ is the standard state concentration taken as 1 M. $\sigma_s$, $\tau_{tun}$, and $\Delta G_f^{\ddagger}$ are the symmetry factor, the tunneling factor, and the forward Gibbs free energy barrier for the reaction, respectively. Tunneling factor is calculated using the Wigner approach [49]. Kinetics-based rate constant for the backward reaction can be expressed similarly by using Gibbs free energy in the backward direction $\Delta G_b^{\ddagger}$. The kinetics-based rate constant accounts for the energy required to cross the activation barrier but does not consider the finite time required for the molecules to diffuse through the solution. The rate at which molecules diffuse to react with one another depends on their size and solution viscosity. As viscosity of the solution increases, the diffusion of molecules within the solution decreases. As a result, the reaction rate is limited by the diffusion process for otherwise kinetically fast reactions. For kinetically slow reactions, diffusion has a negligible or no effect at all.

The mathematical treatment used here for consideration of diffusion represents an extension of theory for bimolecular reactions with neutral species provided by Strehlow [50]. For a general elementary reaction of the form, $A + B + \ldots \leftrightarrow P + Q + \ldots$, diffusion of the reactants to form a reactant complex can be approximated by sequential combination of these species. Similarly, the diffusive dissociation of product complex to form all the products can be approximated by its sequential dissociation. The diffusion rate constants for these intermediate steps are given by [50],

$$k_{diff,c} = 4\pi N_A\ R(D_p + D_Q) \text{ and } k_{diff,d} = 4\pi R(D_p + D_Q)/V. \tag{5}$$

$k_{diff,c}$ is diffusion rate constant for combination of species $P$ and $Q$, whereas $k_{diff,d}$ is the diffusion rate constant for dissociation of $PQ$. $N_A$ is Avogadro number, R is encounter radius, $V$ is volume corresponding to encounter radius, and $D$ is diffusion coefficient. Diffusion coefficient is inversely proportional to molecule radius $r$ and is given by $D = k_B T/6\pi\eta r$ where $\eta$ is dynamic viscosity of the solution. The net diffusion rate constants in forward and backward directions can be obtained by applying quasi-static assumption. The radius of each molecule is approximated according to the method used in computing its volume within the Gaussian program package. The viscosity of the solution is approximated by viscosity of RDX at the solution temperature. For RDX, viscosity was calculated at various temperatures using equilibrium molecular dynamics calculation and then fitted to a cubic polynomial for 475–675 K range,

$\eta = \quad (-\ 0.002551883266\ T^3 + 5.1897440080\ T^2 -\ 3531.527767\ T + 807,165.85) \times 10^{-6}$ Pa-s.

### 5.3. Analysis of gas-phase region

The gas-phase model is also based on the conservation equations of mass and species. The gas-phase CV is shown in Fig. 1. Decomposition products which evaporate from the liquid phase mix with the purge gas in this CV. Uniform mixing of the species is assumed and hence the gas-phase model is also zero-dimensional. The gaseous mixture leaves the CV to the large volume of the thermolysis chamber. For this open CV, a constant pressure of 1 atm is reasonable. The purge gas is at room temperature and hence, temperature of the decomposition products decreases as they mix with it. It is suitable to assume that chemical reactions cease to occur in gas-phase CV. For high flow rate of purge gas, temperature inside the CV remains constant. Ideal gas law is applicable for the gaseous mixture.

Under these model assumptions, the mass conservation equation for species $i$ in terms of its mole fraction $X_{g,\,i}$ in gas-phase region with $n_g$ species is given by,

$$\frac{d}{dt}\left(X_{g,i}\right) = \frac{R_u\ T}{P\ V_g\ W_i}\left[m_{l,T}Y_{l,i}k_{lg,i} - \left(\sum_{j=1}^{n_g-1}\frac{m_{l,T}Y_{l,j}k_{lg,j}}{W_j} + \frac{\dot{m}}{W_P}\right)X_{g,i}W_i\right],$$
$$i = 1,\ 2,\ \ldots,\ n_g - 1 \tag{6}$$

where, $P$ and $V_g$ are pressure and volume of the gas-phase CV, respectively.

The mass conservation equation for the purge gas in terms of its mole fraction $X_{g,\,P}$ is given by,

$$\frac{d}{dt}\left(X_{g,P}\right) = \frac{R_u\ T}{P\ V_g\ W_P}\left[\dot{m}_P - \left(\sum_{j=1}^{n_g-1}\frac{m_{l,T}Y_{l,j}k_{lg,j}}{W_j} + \frac{\dot{m}}{W_P}\right)X_{g,P}W_P\right] \tag{7}$$

where, $W_P$ is molecular weight of purge gas.

Note that energy conservation equation is not required in the model. Experimentally obtained temperature variation is provided as input to the model, described by Eq. (1). A constant temperature of 200°C is considered for gas phase. Eqs. (2), (6), and (7) together form a system of first-order differential equations. With the availability of a comprehensive reaction mechanism, these differential equations are solved simultaneously to obtain the temporal variation of species mole fractions in both liquid-phase and gas-phase regions. The initial conditions used are (1) mole fraction of RDX in liquid-phase CV is 1 at $t = 0$ and (2) mole fraction of purge gas in gas-phase CV is 1 at $t = 0$. The decomposition mechanism for RDX has reactions with a wide range of time scales, producing a stiff system of first-order differential equations. This stiff system of equations is solved using the DVODE routines developed by Brown et al. [51]. The routines use multistep methods with fully variable time steps and outperform fixed-step-interpolatory methods on problems with widely different active time scales [51].

## 6. Computational results and comparison with experiments

Using the method explained in Section 5.1, a total of 500 elementary liquid-phase reactions describing decomposition of RDX were identified. These reactions include 321 species and have molecularity between 1 and 3. This reaction mechanism is provided as Supplementary Material. Along with these reactions, the developed reaction mechanism also includes data required for estimating reaction rates, including the imaginary frequency of the transition state for computing the tunneling factor using the Wigner approach [49], as well as forward and backward free energy and enthalpy of transition state for each reaction.

### 6.1. Parameter optimization

The computational model was simulated for various set temperatures at a constant gas-phase pressure of 1 atm. The variation of evaporation rates of different species with temperature is not available in the literature, and hence liquid-to-gas conversion rates were optimized using experimental results of CRT. Out of the 321 species present in the liquid phase, 24 species were considered to evaporate. These species were selected on the basis of molecular weight and relative concentration in the liquid phase. The liquid-to-gas conversion rates are expressed in an Arrhenius form. The initial guesses for the pre-exponential factors and the activation energies for evaporation were based on a previous study on hydroxylammonium nitrate by Lee and Litzinger [42]. The fitted values obtained by the optimization process are provided in Table S2 of the supplementary material.

The parameters specified in the reaction mechanism also have inherent error ranges associated with them. The error ranges depend upon the level of theory used for the QM calculations, but more importantly on the solvation model itself. The calculated forward and backward free energy barriers in liquid phase have an estimated uncertainty up to 4-5 kcal/mol. Using the computational model, these free energy barrier values were optimized with the guidance from the experimental results of CRT. Sensitive reactions were identified by performing sensitivity analysis. The first-order sensitivity coefficient was defined as the ratio of change in evolved species mole fractions with change in forward and backward activation barriers of a reaction [18]. The free energy barriers of the sensitive reactions were modified by a maximum of 3.8 kcal/mol. Optimized free energy barriers for sensitive reactions are provided in Table S3 of the supplementary material.

### 6.2. Validation of the detailed reaction mechanism

Figure 5 shows the relative mole fractions of evolved gases in gas-phase region obtained experimentally and computationally for a set temperature of 538 K. In the experimental results, non-zero values of the relative mole fractions are only obtained after approximately 0.5 s. This delay in the evolution of gases is caused by the slow initiation of RDX decomposition at 538 K, finite rate of increase of temperature, and the time required for gases to leave the thermolysis region. The computational model takes into account the RDX decomposition rate and temporal variation of sample temperature but assumes that the gaseous products instantly escape from the thermolysis region. Hence, the peaks in evolution profiles are slightly shifted early in time in the computational result.

For a given set temperature, the magnitude of the relative mole fractions depends upon the initial mass of RDX sample. Hence, the trend of relative mole fractions should be compared instead of the absolute values. The experimental results shown in Fig. 5 reveal that the relative mole fraction of $NO_2$ increases rapidly during the initial decomposition phase and then decreases. This trend is successfully captured by the model. However, the model predicts a slightly early peak in $NO_2$ profile compared to experimental result. The experimentally obtained profiles of NO and $NO_2$ are similar with lower relative mole fraction values for NO. This similarity in NO and $NO_2$ profiles is also captured by the computational model. In both experimental and computational results, the initial evolution of $N_2O$ and $CH_2O$ is slow compared to $NO_2$. For the later part of the decomposition process, however, their relative mole fractions are higher compared to $NO_2$. The computational evolution profile of $H_2O$ lies within the experimental fluctuation range. The relative mole fractions of HCN, $CO_2$, and CO are small compared to other identified species in the experiments. A reasonable agreement in the evolution trends of these species is obtained by the computational model. HCN relative mole fraction almost matches

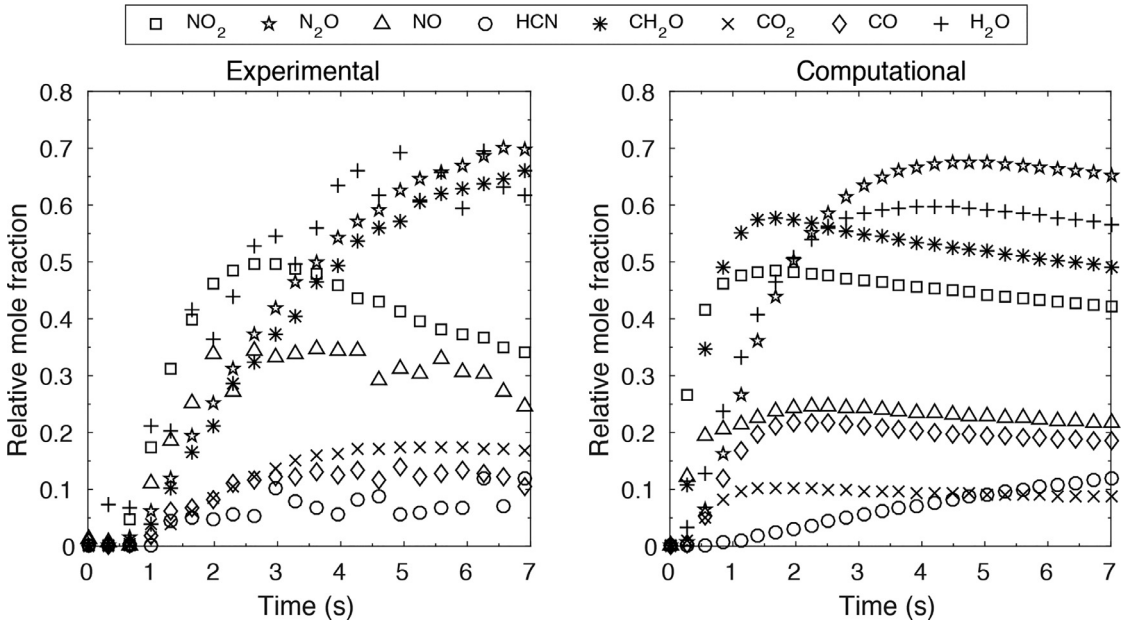


**Fig. 5.** Experimental and computational species evolution profiles in gas phase for RDX decomposition at a set temperature of 538 K.

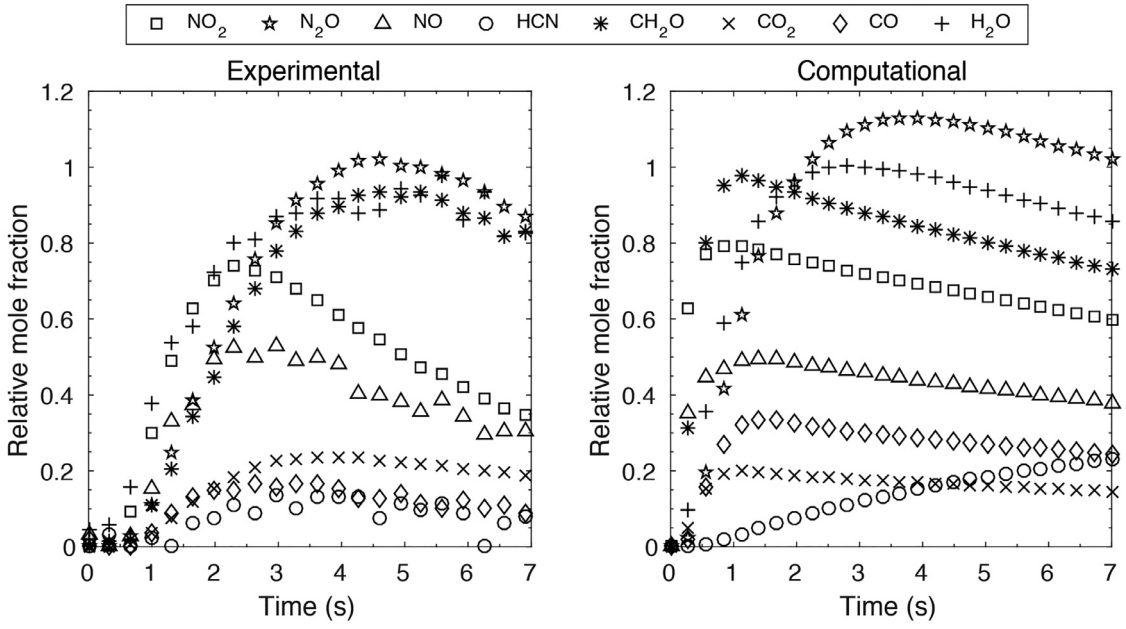


**Fig. 6.** Experimental and computational species evolution profiles in gas phase for RDX decomposition at a set temperature of 548 K.

perfectly whereas CO and $CO_2$ are predicted slightly higher and lower, respectively. The deviation can be justified by the uncertainty in the experimental results, discussed in Section 4.3. The computational model also predicts the mass fraction of RDX remaining at the end of 7 s period in liquid-phase region. For the set temperature of 538 K, the decomposition process is slow and 83.39 percent of RDX compared to its initial mass remains at the end of 7 s.

Figures 6–8 show the comparison between experimental and computational model results for set temperatures of 548 K, 558 K, and 568 K, respectively. The peaks in relative mole fraction profiles occur earlier in time as the set temperature increases. The computational model is able to capture this shift in peaks. The increase in decomposition rate with temperature can be realized by comparing the amount of RDX left in liquid phase after 7 s. The percentages of RDX remaining compared to its initial mass for the set temperatures of 548 K, 558 K, and 568 K are 72.42, 56.6, and 36.8, respectively. Similar to the results for the 538 K set temperature, the experimental trends of relative mole fraction profiles are captured with reasonable accuracy. Although, in general, the predictive capability of the computational model decreases with increasing set temperature. This is likely caused by an increase in experimental uncertainties at higher temperatures, where the gas evolution becomes very rapid.

### 6.3. Reaction mechanism reduction

The results of sensitivity analysis were used to remove unimportant reactions in order to develop a reduced mechanism. The computationally obtained species evolution profiles remain largely

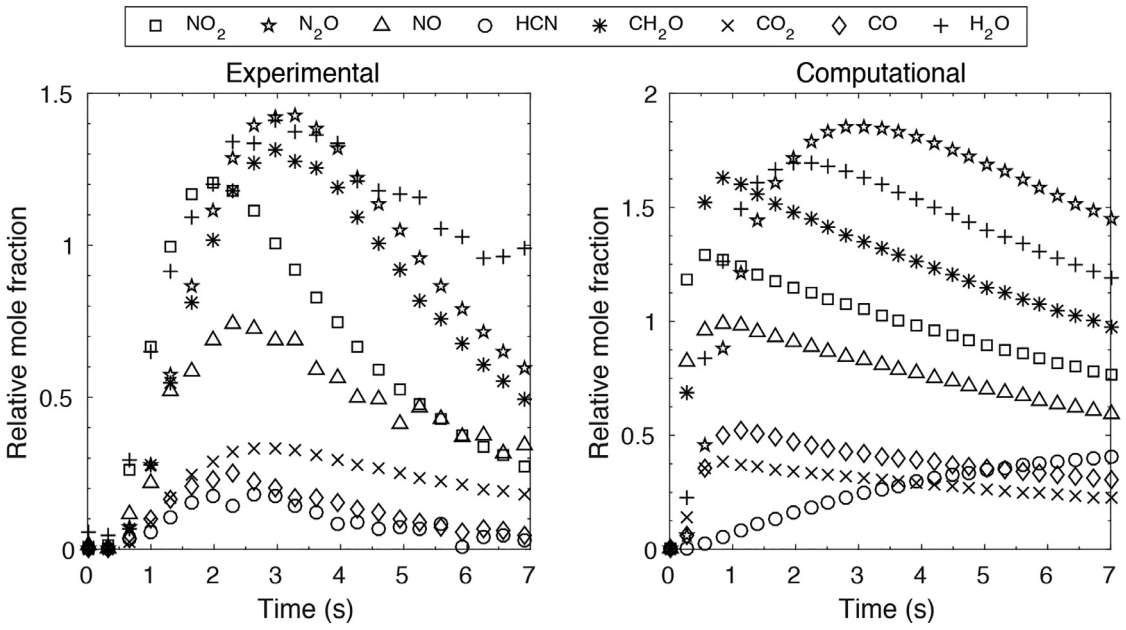


**Fig. 7.** Experimental and computational species evolution profiles in gas phase for RDX decomposition at a set temperature of 558 K.

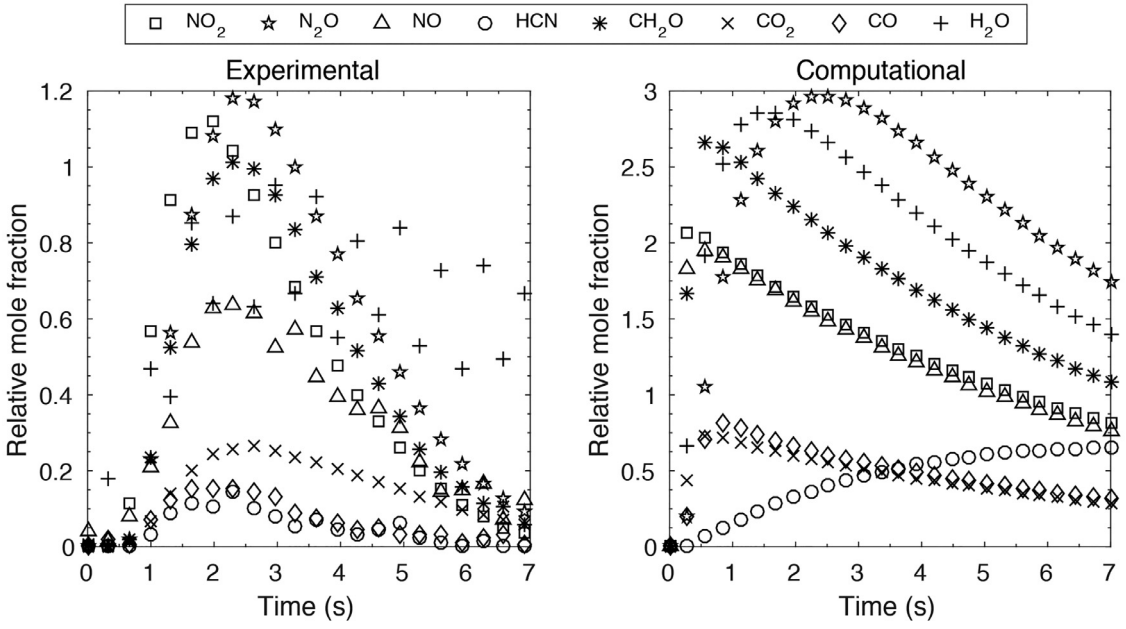


**Fig. 8.** Experimental and computational species evolution profiles in gas phase for RDX decomposition at a set temperature of 568 K.

unchanged when using the reduced mechanism; the deviation is limited to about 1%. But the computational time decreases by a factor of 18 when the reduced mechanism is used instead of the complete mechanism. The reduced mechanism is provided in Table S3. Reactions R1–R34 constitute a set of significant pathways which describes decomposition of RDX into its decomposition products. The important secondary reactions between smaller molecular weight species are listed as R35–R56. The reactions without known transition states are marked with an asterisk (R*). For such reactions, enthalpy of activation is used instead of Gibbs free energy of activation in Eq. (4) for rate calculation [52]. The reduced mechanism represents isothermal decomposition of a small amount of RDX with rapid evolution of products into the surrounding purge gas. As such, the reduced mechanism is not likely to represent the situation of combustion of RDX, in which the temperature varies at high rates and product species have an insufficient time to enter bubbles in a foam layer.

### 6.4. Discussion of the reaction mechanism

The overall reaction mechanism for liquid phase has four initiation steps, (P1) HONO elimination, (P2) $NO_2$ homolytic cleavage, (P3) hydrogen abstraction, and (P4) substitution of nitro group with nitroso group. Based on the values of the forward and reverse activation barriers, Patidar and Thynell [28] proposed HONO elimination as the dominant liquid-phase initiation step. Results show that concentrations of decomposition product species are indeed most sensitive to the HONO elimination step. Other pathways were found to be comparatively much less sensitive. Similar result for gas-phase decomposition was obtained by Chakraborty et al. [53].

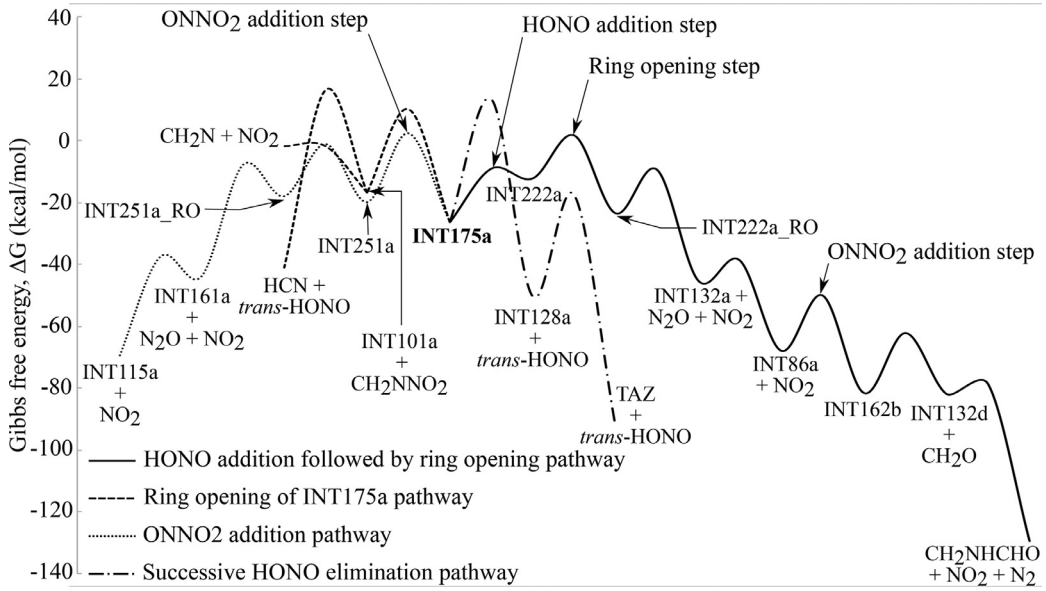


**Fig. 9.** Important pathways for decomposition of INT175a, an intermediate produced by HONO elimination from RDX.

Our proposed dominant initiation step satisfies all the characteristics of rate controlling mechanistic step obtained using deuterium kinetic isotope effect (DKIE) based studies [54,55]. Shackelford et al. [54] found that rate controlling step for RDX decomposition has a covalent carbon-hydrogen bond rupture. Oxley at al. [55] found that RDX dominant decomposition reaction is unimolecular, and has intramolecular hydrogen transfer. Since, HONO elimination is a unimolecular reaction with intramolecular hydrogen transfer, we believe that it is the rate controlling step discussed by Shackelford et al. [54] and Oxley et al. [55]. Oxley et al. [55] also found that mononitroso derivatives are present in much less concentrations during liquid-phase decomposition of RDX. Mononitroso derivatives are formed by the initiation step (P4) which, according to our sensitivity analysis results, is not important in the liquid phase. It should be noted that our result on significance of the initiation step (P4) defer from previous study by Behrens and Bulusu [30]. We believe, the difference in results is potentially due to the occurrence of gas-phase decomposition reactions in their reaction cell. It is also of interest to note that unlike in gas phase where $NO_2$ homolytic cleavage is believed to be a dominant initiation step [11,39,56–58], such initiation is not important in the liquid-phase decomposition. In a recent study on RDX decomposition pathways, a well-defined transition state for $NO_2$ homolytic cleavage in gas phase was located using coupled-cluster theory [59]. Based on the activation barrier values, HONO elimination was proposed as a preferred initiation step over $NO_2$ homolytic cleavage.

The reduced reaction mechanism has four significant pathways for the decomposition of INT175a, which is produced from the HONO elimination initiation step: (P1.1) HONO addition followed by ring opening, (P1.2) ring opening of INT175a, (P1.3) $ONNO_2$ addition, and (P1.4) successive HONO elimination. These pathways are numbered in order of their significance in the liquid phase with P1.1 as the most significant and P1.4 as the least significant pathway. Figure 9 shows the Gibbs free energy profiles for these pathways. Molecular structures of different intermediates formed along these pathways are shown in Fig. S1 of the supplementary material. Sensitivity analysis shows that pathway (P1.1) is responsible for formation of most of the decomposition products in the liquid phase. Pathway (P1.3) has second lowest barrier but due to the insufficient concentration of $ONNO_2$, it becomes much less important. Pathway (P1.2) and pathway (P1.4) have relatively higher barriers and do not contribute towards formation of significant amount of decomposition products.

The decomposition pathway comprises of reactions R1 and R9-R21 of Table S3. The decomposition process initiates via unimolecular HONO elimination, followed by HONO addition in a different configuration. The intermediate thus formed (INT222a) undergoes a ring-opening step followed by two successive unimolecular dissociation steps releasing $NO_2$ and $N_2O$. At this stage, $ONNO_2$ addition takes place which is followed by two successive unimolecular dissociation steps forming $CH_2NHCHO$, $CH_2O$, $NO_2$ and $N_2$. Formation of $N_2$ is responsible for most of the exothermicity observed during RDX decomposition in liquid phase [60]. Further dissociation of $CH_2NHCHO$ occurs via two successive hydrogen-abstraction steps followed by $NO_2$ addition and two successive unimolecular dissociation steps. The various smaller molecular weight species formed along this primary decomposition pathway react with each other to form final decomposition products in experimentally observed composition.

Attempts have also been made to identify competitive pathways where the initiation step is a bimolecular reaction involving RDX. It is driven by the need to simulate reactions during detonation, where the pressure may reach or exceed 20 GPa. For such pressures, Schweigert [61] has used combined molecular dynamics simulations and DFT calculations to identify the reaction

$$RDX + RDX = RDX_{-HONO} + RDX_{+H} + NO_2 \quad \text{(R57)}$$

as having a rate constant greater than the HONO elimination step. At such high pressures, it is expected that rate constants for bimolecular reactions are, in general, larger than for unimolecular reactions [62–64]. The reason is that the activation volume decreases as the pressure increases for bimolecular reactions, whereas the opposite occurs for unimolecular reactions. For the above reaction (R57), we have identified a forward free energy barrier of 56.1 kcal/mol, which suggests that the reaction (R57) is not important for our low-pressure calculations. Factors like viscosity, density, and symmetry could also play an important role, but it is highly doubtful that the rate becomes competitive with the HONO elimination step for pressures applicable to rocket motor conditions. The reaction does, however, satisfy the DKIE effect observed for RDX decomposition [54,55].

The decomposition process of RDX at high pressures (> 0.1 GPa) is far from well understood. Various different decomposition routes have been suggested based on experimental [65–70] and computational studies [64] but consensus has not been achieved. Simultaneous elimination of three HONO molecules from RDX was proposed as a dominant decomposition step in the pressure range 0.2–1.2 GPa by Brower and coworkers [66,67]. Gupta and coworkers [64,68] proposed N–N homolytic cleavage and HONO elimination in 7-10 GPa range, whereas bimolecular reactions were suggested for pressures greater than 10 GPa. RDX decomposition rate also shows an anomalous behavior with pressure and crystal orientation [65,70], which is not observed for its closely related cyclic nitramine, HMX [71]. Hence, there is a need to further investigate RDX decomposition at high pressures where factors such as viscosity and solution density can play a significant role in selection of the preferred decomposition pathway.

## 7. Summary and conclusions

In this study, an expanded version of a recently developed reaction mechanism describing liquid-phase decomposition of RDX was validated using results from CRT. The developed mechanism consists of 321 species and 500 elementary reactions identified using DFT based calculations at B3LYP/6-311++G(d,p) level of theory and the CPCM solvation model. A computational model based on conservation equations was developed. The model uses the reaction mechanism as input and predicts the mole fractions of decomposition products in both liquid and gas-phase regions. Using the experimental data obtained in the gas phase, the reaction rate parameter values were optimized. With the optimized parameters, the computational model captures the experimentally observed trends, in general. This indicates that the proposed reaction mechanism includes most of the key decomposition reactions of RDX in liquid phase. Using sensitivity analysis, a reduced mechanism with 56 elementary reactions and 53 species was also generated.

Out of the four previously known liquid-phase initiation steps, HONO elimination was found to be a dominant decomposition step. Four important pathways were identified for decomposition of HONO elimination product of RDX, (P1.1) HONO addition followed by ring opening, (P1.2) ring opening of INT175a, (P1.3) $ONNO_2$ addition, and (P1.4) successive HONO elimination. Based on our computational model and sensitivity analysis results, we believe that in liquid-phase most of the RDX decomposes via HONO elimination step followed by pathway (P1.1). We also found that, unlike in the gas phase, N–N homolytic cleavage is a minor decomposition pathway in the liquid phase.

Finally, our proposed liquid-phase decomposition mechanism for RDX monopropellant should be valid for operating pressures applicable to rocket motors. Since the mechanism was reduced using results from CRT experiments, one should be careful while using it in combustion models where many complex physiochemical processes occur. For high pressures relevant to detonation, additional bimolecular reaction pathways are likely to play a significant role and our liquid-phase decomposition mechanism in its current state could be used as a starting point for further reaction pathway development.

## Acknowledgments

This material is based upon work was supported by, or in part by, the U.S. Army Research Laboratory and the U.S. Army Research Office under grant number W911NF-15-1-0202.

## Supplementary materials

Supplementary material associated with this article can be found, in the online version, at doi:10.1016/j.combustflame.2018.10.005.

## References

[1] M.W. Beckstead, K. Puduppakkam, P. Thakre, V. Yang, Modeling of combustion and ignition of solid-propellant ingredients, Prog. Energy Combust. Sci. 33 (2007) 497–551.
[2] K.K. Kuo, Chemistry of Nitrate Ester and Nitramine Propellants, Fundamentals of Solid-Propellant Combustion, Progress in Astronautics and Aeronautics, 1984, pp. 177–237, doi:10.2514/5.9781600865671.0177.0237.
[3] S.A. Liebman, A.P. Snyder, J.H. Kremer, D.J. Reutter, M.A. Schroeder, R.A. Fifer, Time-resolved analytical pyrolysis studies of nitramine decomposition with a triple quadrupole mass spectrometer system, J. Anal. Appl. Pyrol. 12 (1987) 83–95.
[4] A.P. Snyder, J.H. Kremer, S.A. Liebman, M.A. Schroeder, R.A. Fifer, Characterization of cyclotrimethylenetrinitramine (RDX) by N, H isotope analyses with pyrolysis–atmospheric pressure ionization tandem mass spectrometry, J. Mass Spectrom. 24 (1989) 15–21.
[5] M.A. Schroeder, Critical analysis of nitramine decomposition data: product distributions from HMX and RDX decomposition, Technical Report BRL-TR-2659 (1985).
[6] C.F. Melius, Thermochemical modeling: II. Application to ignition and combustion of energetic materials, in: Bulusu S.N. (Ed.), Chemistry and Physics of Energetic Materials. NATO ASI Series (Series C: Mathematical and Physical Sciences), 309, Springer, Dordrecht, 1990, pp. 51–78.
[7] J.A. Miller, M.C. Branch, W.J. McLean, D.W. Chandler, M.D. Smooke, R.J. Kee, The conversion of HCN to NO and $N_2$ in $H_2-O_2-HCN-Ar$ flames at low pressure, Symp. (Int.) Combust. 20 (1) (1985) 673–684, doi:10.1016/S0082-0784(85)80557-9.
[8] P. Glarborg, J.A. Miller, R.J. Kee, Kinetic modeling and sensitivity analysis of nitrogen oxide formation in well-stirred reactors, Combust. Flame 65 (1986) 177–202.
[9] J.A. Miller, J.V. Volponi, J.L. Durant, J.E.M. Goldsmith, G.A. Fish, R.J. Kee, The structure and reaction mechanism of rich, non-sooting $C_2H_2/O_2/Ar$ flames, Symp. (Int.) Combust. 23 (1) (1991) 187–194, doi:10.1016/S0082-0784(06)80258-4.
[10] M.H. Alexander, P.J. Dagdigian, M.E. Jacox, C.E. Kolb, C.F. Melius, H. Rabitz, M.D. Smooke, W. Tsang, Nitramine propellant ignition and combustion research, Prog. Energy Combust. Sci. 17 (1991) 263–296.
[11] R.A. Yetter, F.L. Dryer, M.T. Allen, J.L. Gatto, Development of gas-phase reaction mechanisms for nitramine combustion, J. Propuls. Power 11 (1995) 683–697.
[12] D. Chakraborty, R.P. Muller, S. Dasgupta, W.A. Goddard, A detailed model for the decomposition of nitramines: RDX and HMX, J. Comput. Mater. Des 8 (2001) 203–212.
[13] A.D. Becke, Becke's three parameter hybrid method using the LYP correlation functional, J. Chem. Phys 98 (1993) 5648–5652.
[14] T.A. Litzinger, B.L. Fetherolf, Y. Lee, C.-J. Tangi, C.-J. Tang, Study of the gas-phase chemistry of RDX: experiments and modeling, J. Propuls. Power 11 (1995) 698–703.
[15] R.J. Kee, F.M. Rupley, J.A. Miller, Chemkin-II: a fortran chemical kinetics package for the analysis of gas-phase chemical kinetics, Sandia National Labs., Livermore, CA, USA, 1989.
[16] R.J. Kee, F.M. Rupley, J.A. Miller, The Chemkin thermodynamic data base, Sandia National Labs., Livermore, CA, USA, 1990.
[17] R.J. Kee, G. Dixon-Lewis, J. Warnatz, M.E. Coltrin, J.A. Miller, H.K. Moffat, A fortran computer code package for the evaluation of gas-phase multicomponent transport properties, SAND86-8246, Sandia National Labs., Livermore, CA, USA, 1986.
[18] R.J. Kee, J.F. Grcar, M.D. Smooke, J.A. Miller, E. Meeks, PREMIX: a Fortran program for modeling steady laminar one-dimensional premixed flames, SAND85-8249, 1985, Sandia National Labs., Livermore, CA, USA.
[19] Y.-C. Liau, V. Yang, Analysis of RDX monopropellant combustion with two-phase subsurface reactions, J. Propuls. Power 11 (1995) 729–739.
[20] W.R. Anderson, C.B. Conner, Comparison of gas-phase mechanisms applied to RDX combustion model, Proc. Combust. Inst 32 (2009) 2123–2130.
[21] T.B. Brill, P.J. Brush, D.G. Patil, J.K. Chen, Chemical pathways at a burning surface, Symp. (Int.) Combust. 24 (1992) 1907–1914 Elsevier.
[22] C.M. Tarver, T.D. Tran, Thermal decomposition models for HMX-based plastic bonded explosives, Combust. Flame. 137 (2004) 50–62.
[23] M.L. Hobbs, A global HMX decomposition model, Sandia National Labs., Albuquerque, NM (United States), 1996.
[24] R. Behrens Jr., Thermal decomposition of HMX and RDX: Decomposition processes and mechanisms based on STMBMS and TOF velocity-spectra measurements, in: S.N. Bulusu, Chemistry and Physics of Energetic Materials, Springer, 309, 1990, pp. 347–368.
[25] K. Prasad, R.A. Yetter, M.D. Smooke, An eigenvalue method for computing the burning rates of RDX propellants, Combust. Sci. Technol. 124 (1997) 35–82.
[26] K. Prasad, R.A. Yetter, M.D. Smooke, An eigenvalue method for computing the burning rates of HMX propellants, Combust. Flame. 115 (1998) 406–416.

[27] J.E. Davidson, M.W. Beckstead, Improvements to steady-state combustion modeling of cyclotrimethylenetrinitramine, J. Propuls. Power 13 (1997) 375–383.
[28] L. Patidar, S.T. Thynell, Quantum mechanics investigation of initial reaction pathways and early ring-opening reactions in thermal decomposition of liquid-phase RDX, Combust. Flame. 178 (2017) 7–20.
[29] L. Patidar, M. Khichar, S.T. Thynell, Identification of initial decomposition reactions in liquid-phase HMX using quantum mechanics calculations, Combust. Flame 188 (2018) 170–179.
[30] R. Behrens Jr., S. Bulusu, Thermal decomposition of energetic materials. 3. Temporal behaviors of the rates of formation of gaseous pyrolysis products from condensed phase decomposition of 1,3,5-trinitrohexahydro-s-triazine, J. Phys. Chem. 96 (1992) 8877–8891.
[31] S. Bulusu, R. Behrens Jr., A review of the thermal decomposition pathways in RDX, HMX and other closely related cyclic nitramines, Def. Sci. J. 46 (1996) 347–360.
[32] A. Chowdhury, S.T. Thynell, Confined rapid thermolysis/FTIR/ToF studies of imidazolium-based ionic liquids, Thermochim. Acta 443 (2006) 159–172.
[33] E.S. Kim, H.S. Lee, C.F. Mallery, S.T. Thynell, Thermal decomposition studies of energetic materials using confined rapid thermolysis/FTIR spectroscopy, Combust. Flame 110 (1997) 239–255.
[34] C.F. Mallery, S.T. Thynell, Species and temperature profiles of propellant flames obtained from FTIR absorption spectroscopy, Combust. Sci. Technol. 122 (1997) 113–129.
[35] P.R. Griffiths, J.A. De Haseth, Fourier transform infrared spectrometry, Wiley, 2007.
[36] L.S. Rothman, I.E. Gordon, A. Barbe, D.C. Benner, P.F. Bernath, M. Birk, V. Boudon, L.R. Brown, A. Campargue, J.-P. Champion, The HITRAN 2008 molecular spectroscopic database, J. Quant. Spectrosc. Radiat. Transf. 110 (2009) 533–572.
[37] W.H. Press, B.P. Flannery, S.A. Teukolsky, W.T. Vetterling, numerical recipes in Fortran 90, Cambridge University Press, Cambridge, MA., 1992.
[38] P.J. Linstrom, W.G. Mallard, NIST chemistry webBook, NIST standard reference database number 69, NIST, 2014.
[39] Y. Oyumi, T.B. Brill, Thermal decomposition of energetic materials 3. A high-rate, in situ, FTIR study of the thermolysis of RDX and HMX with pressure and heating rate as variables, Combust. Flame 62 (1985) 213–224.
[40] T.B. Brill, P.J. Brush, Condensed phase chemistry of explosives and propellants at high temperature: HMX, RDX and BAMO, Phil, Trans. R. Soc. Lond. A 339 (1992) 377–385.
[41] T.B. Brill, Connecting the chemical composition of a material to its combustion characteristics, Prog. Energy Combust. Sci. 18 (1992) 91–116.
[42] H. Lee, T.A. Litzinger, Chemical kinetic study of HAN decomposition, Combust. Flame 135 (2003) 151–169.
[43] M.J. Frisch, G.W. Trucks, H.B. Schlegel, G.E. Scuseria, M.A. Robb, J.R. Cheeseman, G. Scalmani, V. Barone, B. Mennucci, G.A. Petersson, H. Nakatsuji, M. Caricato, X. Li, H.P. Hratchian, A.F. Izmaylov, J. Bloino, G. Zheng, J.L. Sonnenberg, M. Hada, M. Ehara, K. Toyota, R. Fukuda, J. Hasegawa, M. Ishida, T. Nakajima, Y. Honda, O. Kitao, H. Nakai, T. Vreven, J.A. Montgomery, J.E. Peralta, F. Ogliaro, M. Bearpark, J.J. Heyd, E. Brothers, K.N. Kudin, V.N. Staroverov, R. Kobayashi, J. Normand, K. Raghavachari, A. Rendell, J.C. Burant, S.S. Iyengar, J. Tomasi, M. Cossi, N. Rega, J.M. Millam, M. Klene, J.E. Knox, J.B. Cross, V. Bakken, C. Adamo, J. Jaramillo, R. Gomperts, R.E. Stratmann, O. Yazyev, A.J. Austin, R. Cammi, C. Pomelli, J.W. Ochterski, R.L. Martin, K. Morokuma, V.G. Zakrzewski, G.A. Voth, P. Salvador, J.J. Dannenberg, S. Dapprich, A.D. Daniels, Ö. Farkas, J.B. Foresman, J.V. Ortiz, J. Cioslowski, D.J. Fox, Gaussian 09, Revision D.01, Gaussian Inc. Wallingford CT, 2009.
[44] K.K. Irikura, R.D. Johnson, Is $^{NO3}$ formed during the decomposition of nitramine explosives? J. Phys. Chem. A 110 (2006) 13974–13978.
[45] M. Cossi, N. Rega, G. Scalmani, V. Barone, Energies, structures, and electronic properties of molecules in solution with the C-PCM solvation model, J. Comput. Chem. 24 (2003) 669–681.
[46] E. Cancès, B. Mennucci, J. Tomasi, A new integral equation formalism for the polarizable continuum model : Theoretical background and applications to isotropic and anisotropic dielectrics, J. Chem. Phys. 107 (1997) 3032.
[47] A.V. Marenich, C.J. Cramer, D.G. Truhlar, Universal solvation modle based on solute electron density and a continuum model of the solvent defined by the bulk dielectric constant and atomic surface tensions, J. Phys. Chem. B 113 (2009) 6378–6396.
[48] H. Eyring, The activated complex in chemical reactions, J. Chem. Phys. 3 (1935) 107–115.
[49] E. Wigner, On the quantum correction for thermodynamic equilibrium, Phys. Rev. 40 (1932) 749.
[50] H. Strehlow, Rapid reactions in solution, VCH Weinheim. 1992.
[51] P.N. Brown, G.D. Byrne, A.C. Hindmarsh, VODE: a variable-coefficient ODE solver, SIAM J. Sci. Stat. Comput. 10 (1989) 1038–1051.
[52] S.M. Senkan, Detailed chemical kinetic modeling: chemical reaction engineering of the future, Adv. Chem. Eng., 1992, pp. 95–196. Elsevier.
[53] D. Chakraborty, R.P. Muller, S. Dasgupta, W.A. Goddard, The mechanism for unimolecular decomposition of RDX (1,3,5-Trinitro-1,3,5-triazine), an ab initio Study, J. Phys. Chem. A 104 (2000) 2261–2272.
[54] S.A. Shackelford, S.L. Rodgers, R.E. Askins, Deuterium isotope effects during RDX combustion: mechanistic burn rate-controlling step determination, Propell. Explos. Pyrotech. 16 (1991) 279–286.
[55] J.C. Oxley, A.B. Kooh, R. Szekeres, W. Zheng, Mechanisms of nitramine thermolysis, J. Phys. Chem. 98 (1994) 7004–7008.
[56] F.C. Rauch, A.J. Fanelli, Thermal decomposition kinetics of hexahydro-1,3,5-trinitro-s-triazine above the melting point: evidence for both a gas and liquid phase decomposition, J. Phys. Chem. 73 (1969) 1604–1608.
[57] J. Batten, D. Murdie, The thermal decomposition of RDX at temperatures below the melting point. I. Comments on the mechanism, Aust. J. Chem. 23 (1970) 737.
[58] I.V. Schweigert, Ab initio molecular dynamics of high-temperature unimolecular dissociation of gas-phase RDX and its dissociation products, J. Phys. Chem. A 119 (2015) 2747–2759.
[59] R.W. Molt, T. Watson, A.P. Bazanté, R.J. Bartlett, N.G.J. Richards, Gas phase RDX decomposition pathways using coupled cluster theory, Phys. Chem. Chem. Phys. 18 (2016) 26069–26077.
[60] G.T Long, Sergey. Vyazovkin, A. Brittany, A. Brems, C.A. Wight, Competitive vaporization and decomposition of liquid RDX, J. Phys. Chem. B 104 (2000) 2570–2574.
[61] I. Schweigert, Bimolecular initial reactions in $\gamma$-RDX, Bulletin of the American Physics Society, APS, Los Angeles, CA, 2018.
[62] K.J. Laidler, Chemical kinetics, 3rd ed., Harper&Row, New York, 1987.
[63] D. Furman, R. Kosloff, F. Dubnikova, S.V. Zybin, W.A. Goddard, N. Rom, B. Hirshberg, Y. Zeiri, Decomposition of condensed phase energetic materials: interplay between uni- and bimolecular mechanisms, J. Am. Chem. Soc. 136 (2014) 4192–4200.
[64] M. Miao, Z.A. Dreger, J.E. Patterson, Y.M. Gupta, Shock wave induced decomposition of RDX: quantum chemistry calculations, J. Phys. Chem. A 112 (2008) 7383–7390.
[65] P.J. Miller, S. Block, G.J. Piermarini, Effects of pressure on the thermal decomposition kinetics, chemical reactivity and phase behavior of RDX, Combust. Flame 83 (1991) 174–184.
[66] D.L. Naud, K.R. Brower, Pressure effects on the thermal decomposition of nitramines, nitrosamines, and nitrate esters, J. Org. Chem. 57 (1992) 3303–3308.
[67] J. Wang, K.R. Brower, D.L. Naud, Evidence of an elimination mechanism in thermal decomposition of hexahydro-1,3,5-trinitro-1,3,5-triazine and related compounds under high pressure in solution, J. Org. Chem 62 (1997) 9055–9060.
[68] J.E. Patterson, Z.A. Dreger, M. Miao, Y.M. Gupta, Shock wave induced decomposition of RDX: time-resolved spectroscopy, J. Phys. Chem. A 112 (2008) 7374–7382.
[69] Z.A. Dreger, Y.M. Gupta, Decomposition of $\gamma$-cyclotrimethylene trinitramine ($\gamma$-RDX): relevance for shock wave initiation, J. Phys. Chem. A 116 (2012) 8713–8717.
[70] Z.A. Dreger, M.D. McCluskey, Y.M. Gupta, High pressure-high temperature decomposition of $\gamma$-cyclotrimethylene trinitramine, J. Phys. Chem. A 116 (2012) 9680–9688.
[71] G.J. Piermarini, S. Block, P.J. Miller, Effects of pressure and temperature on the thermal decomposition rate and reaction mechanism of $\beta$-octahydro-1,3,5,7-tetranitro-1,3,5,7-tetrazocine, J. Phys. Chem. 91 (1987) 3872–3878.